# Reduced Graphene Oxide Electrically Contacted Graphene Sensor for Highly Sensitive Nitric Oxide Detection

**Weiwei Li,[†] Xiumei Geng,[†] Yufen Guo,[†] Jizan Rong,[†] Youpin Gong,[†] Liqiong Wu,[†] Xuemin Zhang,[†] Peng Li,[†] Jianbao Xu,[†] Guosheng Cheng,[†] Mengtao Sun,[‡] and Liwei Liu[†,*]**

[†]Suzhou Institute of Nano-Tech and Nano-Bionics, Chinese Academy of Sciences, Suzhou 215123, People's Republic of China and [‡]Institute of Physics, Chinese Academy of Sciences, Beijing 100190, People's Republic of China

**ABSTRACT** We develop graphene-based devices fabricated by alternating current dielectrophoresis (ac-DEP) for highly sensitive nitric oxide (NO) gas detection. The novel device comprises the sensitive channels of palladium-decorated reduced graphene oxide (Pd-RGO) and the electrodes covered with chemical vapor deposition (CVD)-grown graphene. The highly sensitive, recoverable, and reliable detection of NO gas ranging from 2 to 420 ppb with response time of several hundred seconds has been achieved at room temperature. The facile and scalable route for high performance suggests a promising application of graphene devices toward the human exhaled NO and environmental pollutant detections.

**KEYWORDS:** graphene · nitric oxide · dielectrophoresis · reduced graphene oxide · highly sensitive

Graphene is a single atomic layer of $sp^2$-carbon atoms with two-dimensional hexagonal crystal structure. Large specific surface area and high carrier mobility enable graphene to be a promising application in electricity-based sensors.[1] Graphene-based field-effect transistors (FETs) have been examined using mechanical exfoliated graphene as a sensitive channel, exhibiting the sensing ability of individual $NO_2$ gas molecules.[2] Compared with chemically inert graphene,[2−4] reduced graphene oxide (RGO) being of active sites and function groups has been widely demonstrated to be able to detect $NO_2$,[5,6] $NH_3$,[5] $H_2$[7,8] and organic vapors.[9,10] Efforts have been ongoing to focus on the effects of chemical decoration, reduction degree, and device fabrication of RGO on selectivity, sensitivity, and recovery properties of detector devices.[7,10] There is plenty of room for exploration and improvement in this emerging field of graphene-based sensors.

Nitric oxide (NO) detection plays an essential role in medical applications for its biological functions as a messenger molecule. NO molecules can mediate many bodily functions acting as a neurotransmitter and relaxing blood vessels. The human exhaled NO level in 2 weeks prior to outbreak of asthma is doubly elevated compared to everyday NO level of 7−16 ppb,[11] and the detection of NO is critical for an asthma patient in a hospital and with household monitoring. Despite the elevation before outbreak, the NO concentration is still within a range of a few tens of parts per billion. Thus, highly sensitive and portable detection of NO is urgently required for asthma patients.

Carbon nanotubes (CNTs) have been explored to sense NO gas.[11−15] Star *et al.* developed a functionalized CNT network sensor to detect NO gas indirectly by converting NO to $NO_2$ with $CrO_3$, and the direct detection of NO in such devices showed poor performance due to the weak electron donor nature of NO and the detection ability of CNT network devices.[11] Emerging graphene has attracted increasing attention for detection of NO molecules; furthermore, electrons transfer from NO to graphene, and the weak binding between NO molecules and graphene has been recognized theoretically.[16,17] By contrast with single-walled carbon nanotubes (SWNTs), RGO is readily prepared in large quantities and is well-dispersed in aqueous solution without additional surfactants. Thus, it is significant for both fundamental study and application to explore RGO for the direct detection of NO. However, to our best knowledge, related experimental work about direct sensing NO molecules using graphene-based devices has not been reported so far.

As for device fabrications of carbon nanomaterials, alternating current dielectrophoresis (ac-DEP) provides a simple, scalable, and low-cost method to trap carbon nanotubes and graphene for making electronic devices.[18−22] However, an important

* Address correspondence to lwliu2007@sinano.ac.cn.

Received for review April 18, 2011 and accepted August 11, 2011.

**Published online August 11, 2011**
**10.1021/nn201433r**

drawback of such devices derived from ac-DEP lies in the poor electrical contacts, which result in high resistance between metal electrodes and nanoscale carbon materials owing to sample-on-electrode configuration, as well as the presence of Schottky barriers or residue surfactants.[23]

Here, we fabricate the NO sensor devices using ac-DEP of the palladium-decorated reduced graphene oxide (Pd-RGO) nanosheets with chemical vapor deposition (CVD)-grown graphene electrodes. The highly sensitive, recoverable, and reliable detection of NO gas ranging from 2 to 420 ppb with response time of several hundred seconds has been achieved. We adopt a bulk-phase Pd nanoparticle (NP) decoration of RGO as active channels by a solution chemistry method instead of previously reported Pd NPs merely on the surface of the graphene-based devices by electrochemical or physical deposition.[7,8] The advantages of Pd decoration and CVD-grown graphene contacts of RGO in improving the sensitivity and stability of NO sensors have been revealed by performing comparison experiments of various devices. Highly sensitive graphene-based sensor toward directly detecting nitric oxide (NO) is a very promising application for monitoring respiratory disorders and sensing air pollutants.

## RESULTS AND DISCUSSION

Figure 1 shows the schematic illustrations of the process of Pd-RGO composite preparations (a), the device of Pd-RGO with CVD-grown graphene contacts (graphene-Pd-RGO) fabrication and sensor measurement (b). RGO dispersion samples are synthesized by Li's method[24] through a reduction of graphene oxide (GO), and GO is prepared by a modified Hummer's method[25] (see methods in Supporting Information). Transmission electron microscopy (TEM) image in Figure 2a shows the morphology of the produced RGO sheets resembling a thin wrinkled paper. Ultraviolet−visible (UV−vis) spectroscopy suggests a high degree of reduction of GO (see Supporting Information, Figure S1). TEM image in Figure 2b exhibits that the Pd NPs are decorated onto RGO sheets with nearly homogeneous distribution. Figure 2c shows the high-resolution TEM (HRTEM) image of a single Pd NP with a size of 5 nm, whose lattice spacing of 0.22 nm is in accord with the (111) lattice plane of palladium metal.[26] Sensor devices are fabricated by conventional photolithography and lift-off techniques on $SiO_2$/Si substrates. The nickel electrode patterns are deposited by magnetron sputtering (see details in Supporting Information). The six parallel-plate electrodes in one device are fabricated by a standard lift-off technique, as shown in Figure 2d. The distances of each adjacent pair of electrodes (channel length) are 2, 2, 3, 4, and 5 $\mu$m, respectively.

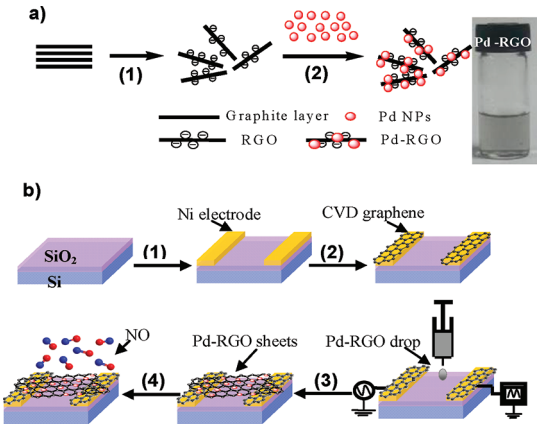


**Figure 1. (a) Schematic illustration of the process for preparation of Pd-RGO composites: (1) RGO synthesis and (2) Pd decoration of RGO. The inset photograph is the diluted Pd-RGO nanosheet suspension used for ac-DEP. (b) Schematics of graphene-Pd-RGO device fabrication and gas sensing test: (1) Ni electrode fabrication, (2) chemical vapor deposition (CVD) growth of graphene, (3) ac-DEP of Pd-RGO nanosheets, and (4) sensor measurement.**

The channel width is 100 $\mu$m (in Figure 2e). To trap the optimal quantity of RGO sheets aligning the electrode and to maintain the consistency of the devices by ac-DEP, we used the devices with the channel length of 3 $\mu$m in our ac-DEP and measurements. The growth of graphene on Ni electrodes is implemented by means of CVD process using methane as a carbon source (see Supporting Information, Figure S2). Raman spectroscopy, scanning electron microscopy (SEM), and TEM (in Figure 2e and Supporting Information, Figure S3) are used to characterize the quality of CVD-grown graphene. Figure 2f (see also in Supporting Information, Figure S4b) shows the SEM image of a Pd-RGO device with CVD-grown graphene electrodes (device A, graphene-Pd-RGO). Two other kinds of devices are fabricated as the control. One kind of device based on bare RGO is fabricated by keeping the conditions of the CVD graphene electrodes, annealing, and ac-DEP the same as the device A except for Pd decoration (device B, graphene-RGO). The other are the devices of Pd-RGO nanosheets assembled by ac-DEP on bare nickel electrodes without CVD-grown graphene covering, while keeping the conditions of annealing and Pd decoration in the same manner (device C, Pd-RGO). Two-probe technique is employed to measure the conductance of the device, in which the conductive channel is made by ac-DEP.

Figure 3a shows a typical change in conductance normalized by initial conductance ($\Delta G/G$) with time, when device A is exposed continuously to five short pulses of NO gas with the time duration of 1, 10, 60, 120, and 240 s corresponding to the concentration of 2, 22, 132, 264, and 528 ppb in a homemade vacuum-sealed stainless steel chamber, respectively. The NO pulses are applied successively on top of the previous

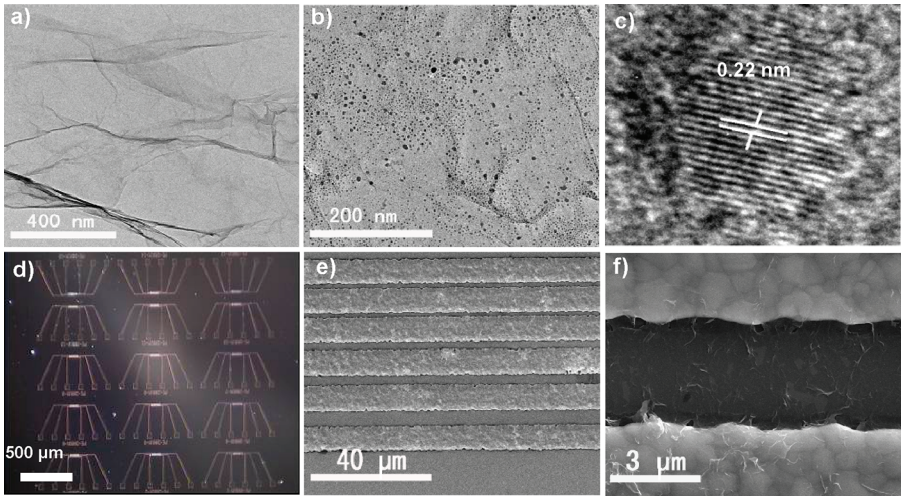


**Figure 2. (a) Transmission electron microscopy (TEM) images of typical graphene sheets and (b) Pd-RGO sheets. (c) High-resolution TEM (HRTEM) image of a single Pd nanoparticle (NP). (d) Optical microscopy image of the microfabricated parallel plate electrode array. (e) Scanning electron microscopy (SEM) image of electrodes covered by CVD-grown graphene. (f) SEM image of Pd-RGO nanosheets trapped between two graphene-covered electrodes by ac-DEP.**

ones when they arrived at equilibrium. Upon initial 2 ppb NO flowing into the chamber, the conductance of the device immediately increases and subsequently gets close to equilibrium. The response time ($t_0$) is defined by the exponential change, $\Delta G/G \propto A + B \exp(t/t_0)$. The response time of ~265 s is obtained by a well fitting treatment (see Supporting Information Figure S5). The wide measurement range within the limitation of our experimental setup is observed for device A, ranging from 2 ppb up to 1 ppm, with an evident sensitivity of approximately 28%. The increase in conductance is consistent with the explanation that NO acts as a donor molecule. The inset in Figure 3a demonstrates a steady-state $\Delta G/G$ as a function of concentration of NO gas ranging from 2 ppb to 1 ppm corresponding to the five short pulses of NO gas. The sensitivity *versus* the concentration shows a linear trend within the range between 2 and 200 ppb, but it begins to deviate and exhibits saturation trend at higher NO concentration.

To investigate the effects of electrodes covered with CVD-grown graphene, Pd decoration of RGO, and current annealing on sensing properties, we fabricated various kinds of devices containing the devices A, B, C, and D (the current-annealed). To obtain typical results, more than five samples for each type of device are measured toward sensing NO gas within the concentration range of 500 ppb, and the reproducibilities of the devices are presented (see Supporting Information, Figure S6). Figure 3b,c shows some typical comparison results of the four kinds of devices under the four continuous increasing NO gas concentrations of 2, 24, 156, and 420 ppb, respectively.

To reveal the role of CVD-grown graphene, the NO responses of device A and device C are shown in Figure 3b. Upon exposure of an initial 2 ppb NO, the sensitivity of device A, ~7%, is relatively smaller than that of device C, ~9%. However, with increasing NO concentration, the sensitivity of device A gradually exceeds that of the device C and reaches ~20%, which is higher than ~15% of device C at the NO concentration of 420 ppb. Opposite to the change of $\Delta G/G$ at the initial infused concentration, the $\Delta G/G$ of the device with CVD graphene electrodes is gradually larger than that of the device with Ni electrodes at higher NO concentration infused. $\Delta G/G$ should be propositional to the product of the carriers transferred from the absorbed NO gas and the mobility of the devices, $\Delta G/G \propto n_{\text{transferred}} \times \mu_{\text{device}}$. The competitive change with gas concentration here can be understood by the change of $n_{\text{transferred}}$ and $\mu_{\text{device}}$ for the two cases with and without CVD graphene electrodes. For the metal contacts, the maximum change of $\Delta G/G$ at the initial exposure of NO gas is due to the increments of the injected carriers from the contact barriers lowering and the bulk doping, as well as the mobility increased by the doping-induced contact improvement. At the high NO concentration, the increased carriers $n_{\text{transferred}}$ resulting from the dominated bulk doping should be equal for two devices with the different contacts, while the mobility of the device with graphene contacts is larger than that of the device with Ni contacts. Thus, at high concentration, the relative change of $\Delta G/G$ of the device with graphene contacts will be larger than that of the device with Ni contacts. Additionally, we also observe that the results of several measured devices without CVD graphene electrodes vary from device to device, while the devices with graphene electrodes show a good stability and reproducibility (see Supporting Information, Figure S6a,c). These results reveal that CVD-grown

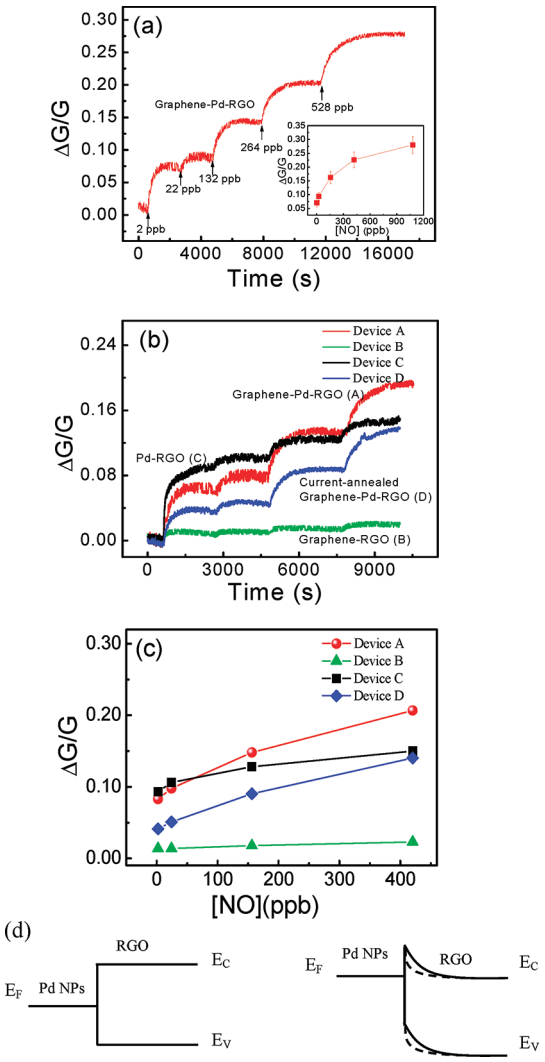


**Figure 3. (a) Relative change in conductance normalized by initial conductance ($\Delta G/G$), real-time sensitivity dependence of device A of graphene-Pd-RGO exposed to several total infused NO gas molecules with the time duration of 1, 10, 60, 120, and 240 s corresponding to the concentrations of 2, 22, 132, 264, and 528 ppb, respectively. The inset demonstrates steady-state $\Delta G/G$ *versus* the concentrations of total infused NO gas molecules ranging from 2 ppb to 1 ppm. (b) Typical relative changes in conductance of the various devices *versus* time, and the step-shaped conductance response corresponds to 1, 10, 60, and 120 s pulses of NO gas: 2, 22, 132, and 264 ppb, respectively. (c) Sensitivities *versus* the total infused concentrations of NO gas in (b). The various devices are device A (graphene-Pd-RGO, red curve), B (graphene-RGO, green curve), C (Pd-RGO, black curve), and D (current-annealed graphene-Pd-RGO, blue curve). (d) Schematic illustrations of the proposed mechanism for sensitivity improvement of the devices due to the Pd NP decorations of RGO. When the device of Pd-RGO was exposed to NO gas, the original symmetric Schottky barriers at the contacts of Pd NPs and RGO (left) are transferred to asymmetric n-type Schottky barriers (right) for the electron doping by NO gas. With the doping concentration increasing, the width of the Schottky barrier will be further reduced (right, dashed line).**

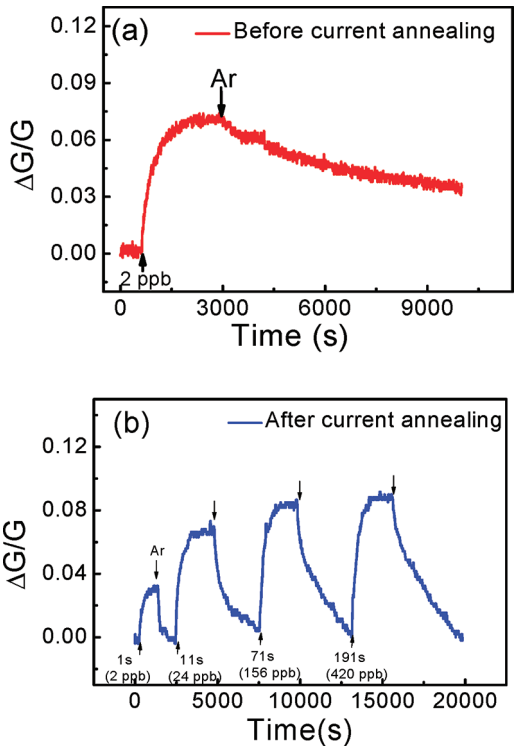


**Figure 4. Comparison of the recovery time of the device A (before current annealing) and device D (after current annealing). The time dependence sensitivities of the devices exposed to 2 ppb NO gas for device A (a) and 2, 24, 156, and 420 ppb for device D (b). Ultrapure Ar is used to desorb the NO absorbed on the device (down arrow). After current annealing on device A, the recovery time is evidently shortened and the sensitivity is lowered.**

graphene electrodes play a critical role in improving the contacts of RGO nanosheets, thereby elevating significantly the stability and consistency of devices. The degraded stability and consistency of the devices without graphene electrodes can be attributed to the geometry configuration of the Pd-RGO nanosheets on Ni electrodes made by ac-DEP. The initial higher sensitivity for stable devices without graphene electrodes can be understood considering the presence of the larger Schottky barriers between Ni and Pd-RGO than that between graphene and Pd-RGO due to the difference of work functions. The relative change in conductance is raised by the reduction of the thickness of Schottky barriers at the very beginning of exposure to NO gas, where the work function of the metal electrodes is easily changed by the initial adsorption of gas molecules. With increasing concentration of NO, the response of intrinsic bulk Pd-RGO would gradually dominate over the contact effect of the metal electrodes. The scattering of the thickness-reduced barriers is responsible for the excess sensitivity by the devices with graphene electrodes. By contrast, the CVD-grown graphene electrodes have similar geometry configuration and work function with RGO, resulting in relatively trivial influence of contacts between CVD graphene electrodes and RGO. This contributes to

the enhancements of the intrinsic response and retains a good stability and consistency of the devices.

In order to illustrate the influence of Pd decoration of RGO on NO gas response sensitivities, two kinds of sensor devices using CVD-grown graphene contacts are investigated, the device A with Pd decoration and the device B without Pd decoration of RGO, respectively. A rather small sensitivity for the device B (~1.3%, green curves) is shown in Figure 3b,c at the concentration of 2 ppb NO gas, and even with the concentration of NO rising to 420 ppb, the sensitivity is only ~2.5%. By contrast, the sensitivity of device A (red curves) is ~7%, which is more than 5-fold of device B when exposed to 2 ppb NO gas and approaches about 9 times higher sensitivity than that of device B at the concentration of 420 ppb. To understand the role of Pd decoration, we assume the presence of symmetric Schottky barriers at the contacts of Pd NPs and intrinsic RGO, locally distributed on the surface of RGO (left in Figure 3d). When the device of Pd-RGO is exposed to the NO gas, the absorption of NO gas molecules takes place on both Pd NPs and RGO. The n-type Schottky barriers would be formed when considering the NO gas electron doping of RGO from NO gas. On the other hand, the work function of Pd NPs is lowered due to the electron transferred from NO gas molecules, and thereby asymmetric n-type Schottky barriers are formed (right in Figure 3d, solid line). With the doping concentration increasing, the width of Schottky barrier will be reduced, which is favorable for the electron transfer from Pd NPs and the enhancement of the conductance (right in Figure 3d, dashed line). Thus, Pd NP decoration of RGO promotes the electron donation from NO into RGO. Pd NPs might play the roles in acting as a absorption medium of NO molecules,[27] the formation of the potential barriers between Pd and RGO, and the interaction with defect sites of RGO, which are similar to the situations of carbon nanotubes.[15,28,29]

We proceed to study the improvement in the recovery time of the devices by employing the current annealing of device A, which has been defined as device D. Figure 4 shows that device A has an extremely long recovery time, almost irrecoverable. We apply a medium current of 1 mA for 1 min to device A in order to accomplish a further reduction of Pd-RGO. In Figure 4, in contrast to device A, the recovery time of device D (blue curves) is greatly improved and a ~1000 s recovery time is obtained at 2 ppb NO concentration. At higher concentrations (such as 420 ppb), the device still shows the recoverable behavior; however, it needs longer recovery time (~1 h). The response time of device D is approximately 240 s, similar to that of device A when exposed to 2 ppb NO gas (see Supporting Information, Figure S5b). Although the sensitivity is lowered to ~4% at 2 ppb NO gas, the current annealing provides an effective means of balancing the recovery time and the sensitivity of the device. The current annealing process has been found to further reduce chemical doping and carrier scatterings for graphene.[30−32] Our Pd-RGO nanosheets comprise oxygen-containing groups which contribute to the irreversible sensitivity of the device.[10] After current annealing, the oxygen-containing groups are partially removed, resulting in fast recovery, at the expense of lowering sensitivity for the NO sensing. In addition, we performed the comparison experiments of the successively and nonsuccessively applied NO pulses. It is found that $\Delta G/G$ values are larger at a high concentration of NO gas in the successive case than that in the nonsuccessive case. This suggests the effect of the integration of NO gas (see Supporting Information, Figure S9). Device D is used to detect $NO_2$ and $NH_3$, which are widely considered as hole and electron donor gases, respectively.[5,6] The conductance increases when exposing the device to the both gases, although with a weaker response of $NH_3$ compared to that of $NO_2$ (see Supporting Information, Figure S8). This suggests that our devices show ambipolar characteristics, where the devices work in the off state at zero and low gate voltages. The weaker response of $NH_3$ compared to that of $NO_2$ is attributed to the possible weak absorption of $NH_3$ on RGO and the absence of the enhanced roles from Pd decoration. Our RGO devices are unavailable for FET characterization due to their metal-like nature and assembled thick RGO that screens the charges from the gate. To determine the nature of donor, we also investigate the response of NO gas using the aligned carbon nanotube device that is characterized by a p-type transistor. The p-type carbon nanotube device shows the conductance increment due to the shift and elevation of the FET transfer curves caused by electron doping of NO gas (see Supporting Information, Figure S11). For clarity, the imaginative ambipolar and p-type FETs are schematically illustrated, indicating the cases that the conductance increases with the electron doping near the off state (see Supporting Information, Figure S10).

## CONCLUSIONS

In summary, we have first demonstrated the graphene-based NO sensor devices by ac-DEP of bulk Pd-RGO nanosheets with CVD-grown graphene electrodes. The stable, highly sensitive, and recoverable graphene devices responding directly to the NO gas have been achieved at room temperature. CVD-grown graphene contacts of Pd-RGO improve the stability and sensitivity of the devices due to the reasonable work function matching

between CVD-grown graphene and RGO. The bulk-phase Pd NP decoration of RGO remarkably increases the sensitivity. A mild current annealing for the devices allows us to balance the sensitivity and the recovery time. Therefore, the novel configuration, facile fabrication method, and excellent sensing performance of these devices show a promising application of the graphene-based devices toward sensitive, rapid, and stable detection of the human exhaled NO gas and environmental pollutants.

## MATERIALS AND METHODS

**Material Preparation.** Graphene oxide was prepared from natural graphite powder (300 mesh, Alfa Aesar) by a modified Hummers method.[24] RGO was prepared and dispersed in water using Li's method.[25] To prepare Pd-RGO composites, we first synthesize Pd NPs using sodium tetrachloropalladate ($Na_2PdCl_4$) as the palladium precursor and ethylene glycol as both solvent and reducing agent, and then add Pd NP solution into RGO dispersions under stirring (see details in Supporting Information). The physical absorption method has the advantage of avoiding precipitation resulting from salt effect over the method of adding RGO directly into palladium precursor solution during the synthesis of Pd NPs.

**Device Fabrication.** Sensor devices are fabricated by conventional photolithography and lift-off techniques on silicon substrates capped with 300 nm thick $SiO_2$. The nickel electrode patterns are deposited by a magnetron sputtering. The growth of graphene on Ni electrodes is implemented by means of a CVD process using methane as the carbon source (see Supporting Information, Figure S2). Utilizing ac-DEP with an alternating current voltage of 10 Vpp and a frequency of 10 kHz, we trap the Pd-RGO nanosheets between prefabricated CVD-grown graphene electrodes (channel length 3 $\mu$m). The devices are annealed mildly in flowing $H_2$/Ar ($H_2$ 100 sccm/Ar 100 sccm) at 200 °C for 30 min to remove residual moisture, solvent content, and partially residual oxygen-containing groups. Comparative experiments of assembly of RGO samples have been performed with and without ac-DEP treatment. The ac-DEP shows its advantages in forming the ordered conductive channels between the electrode spacing on the hydrophobic surface of the wafer substrate, while most of the devices made by the drop casting show insulating behavior due to their random distributions over the entire surface of the device. The photographs show the difference of those two methods (see Supporting Information, Figure S3c).

**Material Characterization and Sensing Test.** Raman measurements are carried out using a Labram HR800 UV−NIR from Jobin Yvon with a laser wavelength of 632.8 nm. Transmission electron microscopy (TEM) image was taken on a FEI Tecnai G2F20S-Twin transmission electron microscope at an accelerating voltage of 100 kV. The samples are prepared by dropping 1 $\mu$L of RGO solution onto a microgrid. UV−vis spectroscopy measurements are performed on a RGO aqueous dispersion, using a Perkin-Elmer Lambda 25 spectrophotometer. Scanning electron microscopy (SEM) image was obtained on a Quanta 400 FEG scanning electron microscope.

The gas sensing measurements are performed in a homemade vacuum-sealed stainless steel chamber using an Agilent semiconductor parameter analyzer B1500A. The real-time conductance response of our devices is tested when exposed to different concentrations of NO in pure $N_2$. Ultrapure Ar gas (99.999%) is used for desorption of the adsorbates on the devices for the recovery. Unless noted otherwise, the channel length of the devices is fixed to 3 $\mu$m and all measurements are performed with a source−drain bias of 50 mV at room temperature. We define the sensitivity $S$ of the sensors as the relative change of the conductance, $S = (G_{gas}-G)/G = \Delta G/G \times 100\%$, where $G_{gas}$ is the conductance in NO gas, $G$ is the conductance in vacuum, and $\Delta G$ represents the conductance change upon gas exposure.

*Acknowledgment.* This work was supported by National Natural Science Foundation of China (Grant Nos. 10974141, 90923003). We also acknowledged the funding support by the National Basic Research Program of China (2010CB934700), the Key Program of the National Science Foundation of China (Award ID 10834004), and Suzhou Science and Technology Development Plan. L.W.L. thanks the Platforms of Characterization & Test and Nanofabrication Facility at Sinano for experimental assistance.

*Supporting Information Available:* The detailed description of the Pd-RGO composite synthesis, the device fabrication, and characterization methods, Figures S1−S11. This material is available free of charge *via* the Internet at http://pubs.acs.org.

## REFERENCES AND NOTES

1. Park, S.; Ruoff, R. S. Chemical Methods for the Production of Graphenes. *Nat. Nanotechnol.* **2009**, *4*, 217–224.
2. Schedin, F.; Geim, A. K.; Morozov, S. V.; Hill, E. W.; Blake, P.; Katsnelson, M. I.; Novoselov, K. S. Detection of Individual Gas Molecules Adsorbed on Graphene. *Nat. Mater.* **2007**, *6*, 652–655.
3. Dan, Y. P.; Lu, Y.; Kybert, N. J.; Luo, Z. T.; Johnson, A. T. C. Intrinsic Response of Graphene Vapor Sensors. *Nano Lett.* **2009**, *9*, 1472–1475.
4. Joshi, R. K.; Gomez, H.; Alvi, F.; Kumar, A. Graphene Films and Ribbons for Sensing of $O_2$ in Practical Conditions. *J. Phys. Chem. C* **2010**, *114*, 6610–6613.
5. Fowler, J. D.; Allen, M. J.; Tung, V. C.; Yang, Y.; Kaner, R. B.; Weiller, B. H. Practical Chemical Sensor from Chemically Derived Graphene. *ACS Nano* **2009**, *3*, 301–306.
6. Jeong, H. Y.; Lee, D. S.; Choi, H. K.; Lee, D. H.; Kim, J. E.; Lee, J. Y.; Lee, W. J.; Kim, S. O.; Choi, S. Y. Flexible Room-Temperature $NO_2$ Gas Sensors Based on Carbon Nanotubes/Reduced Graphene Hybrid Films. *Appl. Phys. Lett.* **2010**, *96*, 213105.
7. Sundaram, R. S.; Gómez-Navarro, C.; Balasubramanian, K.; Burghard, M.; Kern, K. Electrochemical Modification of Graphene. *Adv. Mater.* **2008**, *20*, 3050–3053.
8. Johnson, J. L.; Behnam, A.; Pearton, S. J.; Ural, A. Hydrogen Sensing Using Pd-Functionalized Multi-layer Graphene Nanoribbon Networks. *Adv. Mater.* **2010**, *22*, 4877–4880.
9. Dua, V.; Surwade, S. P.; Ammu, S.; Agnihotra, S. R.; Jain, S.; Roberts, K. E.; Park, S.; Ruoff, R. S.; Manohar, S. K. All-Organic Vapor Sensor Using Inkjet-Printed Reduced Graphene Oxide. *Angew. Chem., Int. Ed.* **2010**, *49*, 2154–2157.
10. Robinson, J. T.; Perkins, F. K.; Snow, E. S.; Wei, Z. Q.; Sheehan, P. E. Reduced Graphene Oxide Molecular Sensors. *Nano Lett.* **2008**, *8*, 3137–3140.
11. Kuzmych, O.; Allen, B. L; Star, A. Carbon Nanotubes Sensors for Exhaled Breath Components. *Nanotechnology* **2007**, *18*, 375502.
12. Mäklin, J.; Mustonen, T.; Kordás, K.; Saukko, S.; Tóth, G.; Vähäkangas, J. Nitric Oxide Gas Sensor with Functionalized Carbon Nanotubes. *Phys. Status Solidi B* **2007**, *244*, 4298–4302.
13. Long, R. Q.; Yang, R. T. Carbon Nanotubes as a Superior Sorbent for Nitrogen Oxides. *Ind. Eng. Chem. Res.* **2001**, *40*, 4288–4291.
14. Liang, Y. X.; Chen, Y. J.; Wang, T. H. Low-Resistence Gas Sensor Fabricated from Multiwalled Carbon Nanotubes Coated with a Thin Tin Oxide Layer. *Appl. Phys. Lett.* **2004**, *85*, 666–668.
15. Kauffman, D. R.; Star, A. Chemically Induced Potential Barriers at the Carbon Nanotube−Metal Nanoparticle Interface. *Nano Lett.* **2007**, *7*, 1863–1868.

16. Imani, K.; Abolhassani, M. R.; Sabouri-Dodaran, A. A. Electronic Transport Calculation of Adsorbate $NO_2$ and NO Molecules on Graphene Using Maximally Localized Wannier Functions. *Eur. Phys. J. B* **2010**, *74*, 135–138.
17. Zhang, Y. H.; Chen, Y. B.; Zhou, K. G.; Liu, C. H.; Zeng, J.; Zhang, H. L.; Peng, Y. Improving Gas Sensing Properties of Graphene by Introducing Dopants and Defects: A First-Principles Study. *Nanotechnology* **2009**, *20*, 185504.
18. Blatt, S.; Hennrich, F.; von Lŏhneysen, H.; Kappes, M. M.; Vijayaraghavan, A.; Krupke, R. Influence of Structural and Dielectric Anisotropy on the Dielectrophoresis of Single-Walled Carbon Nanotubes. *Nano Lett.* **2007**, *7*, 1960–1966.
19. Vijayaraghavan, A.; Blatt, S.; Weissenberger, D.; Oron-Carl, M.; Hennrich, F.; Gerthsen, D.; Hahn, H.; Krupke, R. Ultra-Large-Scale Directed Assembly of Single-Walled Carbon Nanotube Devices. *Nano Lett.* **2007**, *7*, 1556–1560.
20. Vijayaraghavan, A.; Sciascia, C.; Dehm, S.; Lombardo, A.; Bonetti, A.; Ferrari, A. C.; Krupke, R. Dielectrophoretic Assembly of High-Density Arrays of Individual Graphene Devices for Rapid Screening. *ACS Nano* **2009**, *3*, 1729–1734.
21. Joung, D.; Chunder, A.; Zhai, L.; Khondaker, S. I. High Yield Fabrication of Chemically Reduced Graphene Oxide Field Effect Transistors by Dielectrophoresis. *Nanotechnology* **2010**, *21*, 165202.
22. Burg, B. R.; Lütolf, F.; Schneider, J.; Schirmer, N. C.; Schwamb, T.; Poulikakos, D. High-Yield Dielectrophoretic Assembly of Two-Dimensional Graphene Nanostructures. *Appl. Phys. Lett.* **2009**, *94*, 053110.
23. Ranjan, N.; Mertig, M. Dielectrophoretically Assembled Carbon Nanotube−Metal Hybrid Structures with Reduced Contact Resistance. *Phys. Status Solidi B* **2008**, *245*, 2311–2314.
24. Li, D.; Müller, M. B.; Gilje, S.; Kaner, R. B.; Wallace, G. G. Processable Aqueous Dispersions of Graphene Nanosheets. *Nat. Nanotechnol.* **2008**, *3*, 101–105.
25. Hummers, W. S.; Offeman, R. E. Preparation of Graphitic Oxide. *J. Am. Chem. Soc.* **1958**, *80*, 1339.
26. Piao, Y. Z.; Jang, Y. J.; Shokouhimehr, M.; Lee, I. S.; Hyeon, T. Facile Aqueous-Phase Synthesis of Uniform Palladium Nanoparticles of Various Shapes and Sizes. *Small* **2007**, *3*, 255–260.
27. Brown, W. A.; King, D. A. NO Chemisorption and Reactions on Metal Surfaces: A New Perspective. *J. Phys. Chem. B* **2000**, *104*, 2578–2595.
28. Khalap, V. R.; Sheps, T.; Kane, A. A.; Collins, P. G. Hydrogen Sensing and Sensitivity of Palladium-Decorated Single-Walled Carbon Nanotubes with Defects. *Nano Lett.* **2010**, *10*, 896–901.
29. Kauffman, D. R; Sorescu, D. C.; Schofield, D. P.; Allen, B. L.; Jordan, K. D.; Star, A. Understanding the Sensor Response of Metal-Decorated Carbon Nanotubes. *Nano Lett.* **2010**, *10*, 958–963.
30. Bolotin, K. I.; Sikes, K. J.; Hone, J.; Stormer, H. L.; Kim, P. Temperature-Dependent Transport in Suspended Graphene. *Phys. Rev. Lett.* **2008**, *101*, 096802.
31. Moser, J.; Barreiro, A.; Bachtold, A. Current-Induced Cleaning of Graphene. *Appl. Phys. Lett.* **2007**, *91*, 163513.
32. Bolotin, K. I.; Sikes, K. J.; Jiang, Z.; Klima, M.; Fudenberg, G.; Hone, J.; Kim, P.; Stormer, H. L. Ultrahigh Electron Mobility in Suspended Graphene. *Solid State Commun.* **2008**, *146*, 351–355.